

A novel metastable structure and superconductivity of hydrogen-rich compound CdH_6 under pressure

Yan Yan(闫岩), Chengao Jiang(蒋成澳), Wen Gao(高稳), Rui Chen(陈蕊), Xiaodong Yang(杨晓东), Runru Liu(刘润茹), Lihua Yang(杨丽华), and Lili Wang(王丽丽)

Citation: Chin. Phys. B, 2025, 34 (**8**): 086201. DOI: 10.1088/1674-1056/add902
http://cpb.iphy.ac.cn; http://iopscience.iop.org/cpb

What follows is a list of articles you may be interested in

Band gap engineering and vibrational properties of van der Waals semiconductor $ZnPSe_3$ under compression

Rouqiong Su(苏柔琼), Yuying Li(李玉莹), Chunhua Chen(陈春华), Yifang Yuan(袁亦方), and Haizhong Guo(郭海中)
Chin. Phys. B, 2025, 34 (**6**): 066205. DOI: 10.1088/1674-1056/adcaa2

Structural regulation and optical behavior of zero-dimensional Cu(I)-based organometallic halides under pressure

Runnan Ye(叶润楠), Jingtian Wang(王敬天), Jiayi Yang(杨佳毅), Xuchen Wang(王旭晨), Junce Lei(雷钧策), Wenya Zhao(赵文雅), Yufan Meng(孟雨凡), Guanjun Xiao(肖冠军), and Bo Zou(邹勃)
Chin. Phys. B, 2025, 34 (**6**): 066204. DOI: 10.1088/1674-1056/adc193

Stoichiometric change and solid decomposition in Ca-S compounds under high pressure

Yang Lv(吕阳), Jian-Fu Li(李建福), Zhao-Bin Zhang(张钊彬), Yong Liu(刘勇), Jia-Nan Yuan(袁嘉男), Jia-Ni Lin(林佳妮), and Xiao-Li Wang(王晓丽)
Chin. Phys. B, 2025, 34 (**4**): 046202. DOI: 10.1088/1674-1056/adb38e

Theoretical insights into the structures and fundamental properties of pnictogen nitrides

Jingjing Wang(王晶晶), Panlong Kong(孔攀龙), Dingmei Zhang(张定梅), Defang Gao(高德芳), Zaifu Jiang(蒋再富), and Wei Dai(戴伟)
Chin. Phys. B, 2024, 33 (**9**): 096201. DOI: 10.1088/1674-1056/ad6a07

High-pressure study on calcium azide ($Ca(N_3)_2$): Bending of azide ions stabilizes the structure

Xiaoxin Wu(武晓鑫), Yingjian Wang(王颖健), Siqi Li(李思琪), Juncheng Lv(吕俊呈), Jingshu Wang(王婧姝), Lihua Yang(杨丽华), Qi Zhang(张旗), Yanqing Liu(刘艳清), Junkai Zhang(张俊凯), and Hongsheng Jia(贾洪声)
Chin. Phys. B, 2024, 33 (**5**): 056201. DOI: 10.1088/1674-1056/ad2b53

SPECIAL TOPIC — Structures and properties of materials under high pressure

A novel metastable structure and superconductivity of hydrogen-rich compound CdH_6 under pressure

Yan Yan(闫岩)[1,†], Chengao Jiang(蒋成澳)[1], Wen Gao(高稳)[1], Rui Chen(陈蕊)[1], Xiaodong Yang(杨晓东)[1], Runru Liu(刘润茹)[1], Lihua Yang(杨丽华)[2], and Lili Wang(王丽丽)[1]

[1] *School of Materials Science and Engineering, Changchun University, Changchun* 130022, *China*

[2] *Key Laboratory of Functional Materials Physics and Chemistry of the Ministry of Education, Key Laboratory of Preparation and Application of Environmental Friendly Materials, College of Physics, Jilin Normal University, Changchun* 130103, *China*

(Received 24 February 2025; revised manuscript received 22 April 2025; accepted manuscript online 15 May 2025)

The particle swarm optimization algorithm has predicted a series of binary cadmium hydrides that could be dynamically stable at pressures between 100 GPa and 300 GPa. These low-energy phases are composed of both Cd atoms and H_2 molecules. Here, we propose a hitherto unknown metastable *Cmcm*-CdH_6 phase, consisting of one-dimensional zigzag graphite-like hydrogenic H_6 chains, quasimolecular H_2 units and Cd atoms, which is metallic above 290 GPa. Due to H_2 $\sigma \rightarrow$ Cd d donation and Cd d $\rightarrow$ H_2 σ^* back-donation, the electrons occupy antibonding orbitals for both types of hydrogen atoms. This results in weakened chemical bonds in the *Cmcm*-CdH_6 phase via a Kubas-like mechanism, promoting the emergence of high superconductivity, which is estimated to be up to $\sim$ 60 K at 290 GPa. This work will inspire the search for superconductivity in materials based on group IIB hydrides under pressure.

Keywords: high pressure, hydrogen-rich compounds, superconductivity

PACS: 62.50.–p, 74.62.Fj, 63.20.kd, 62.20.–x

DOI: 10.1088/1674-1056/add902 **CSTR:** 32038.14.CPB.add902

1. Introduction

The search for room-temperature superconductivity remains one of the greatest challenges in the field of condensed matter physics and materials science.[1–8] Hydrogen is the lightest element in the periodic table. It was found that hydrogen has many significant physical and chemical properties. In particular, Ashcroft predicted that it potentially could become a high- or room-temperature superconductor due to its light weight, high Debye temperature and strong electron–phonon coupling.[9] However, this has not been proven in the maximum range of experimental pressure. Subsequently, Ashcroft said that the addition of another element to hydrogen could decrease its metallic pressure through the so-called 'chemical precompression' method, whilst keeping all of the beneficial properties required for superconductivity.[10–13] Meanwhile, high pressure has been used as an effective route to increase the amount of hydrogen that may be stored in materials and to synthesize novel materials such as high-temperature superconductors. Many new structures can be formed under compression, many of which are hydrogen-rich compounds.[14] The first successful experimental breakthrough in the superconducting field was the report of a superconducting critical temperature T_c value up to 203 K at 155 GPa in the H_3S structure.[2,15] A second class of hydrides with high T_c values, which were initially predicted by first-principles calculations and then synthesized in experiments, are metal superhydrides, including LaH_{10} (250–260 K around 200 GPa),[3,16,17] CaH_6 (215 K at 172 GPa),[5,18–20] ThH_{10} (161 K at 175 GPa),[21] YH_6 (220 K at 166 GPa) and YH_9 (262 K at 182 GPa).[17,22–24] These presented hydrides feature quasimolecular H_2 units and atomic H, as well as extended hydrogenic lattices. Such structural achievements enhanced interest in further searches for possible high- or room-temperature superconducting hydrides.

In this paper, high-pressure structures and the superconductivity of CdH_n (n = 1–7) are investigated by a combination of the particle swarm optimization algorithm and first-principles calculations. Under compression, group IIB elements are expected to transfer electrons to hydrogen atoms occupying their antibonding orbitals, which might include the decomposition of H_2 units and help the formation of hydrides, which have excellent structural characteristics and play an important role in the superconducting transition. Interestingly, a new cadmium hydride, CdH_6, has been described that contains two types of hydrogen atoms which are composed of one-dimensional (1D) zigzag graphite-like hydrogenic H_6 chains and quasimolecular H_2 units.

2. Computational methods

Crystal structure prediction searches were carried out using CALYPSO software[25,26] based on a particle swarm op-

†Corresponding author. E-mail: yanyan1110@126.com

© 2025 Chinese Physical Society and IOP Publishing Ltd. All rights, including for text and data mining, AI training, and similar technologies, are reserved.

timization algorithm in combination with density functional theory (DFT). The details of this search algorithm and its significant applications have been described elsewhere. This method has been used to successfully predict the crystal structures of many functional materials. We performed crystal structure searching of CdH_n (n = 1–7) within the simulation cells of 1–4 formula units at 100 GPa, 200 GPa and 300 GPa, respectively. The structural optimization was performed using DFT with the generalized gradient approximation, as included in the Vienna *ab initio* Simulation Package (VASP) code. The electron–ion interaction was described by means of the projector augmented wave (PAW) method,[27,28] with Cd $4d^{10}5s^2$ and H $1s^1$ treated as the valence electrons, respectively.[29] The plane-wave kinetic energy cutoff was 600 eV for precise optimizations. The dense k-point sampling was generated using the Γ-centered Monkhorst–Pack scheme,[30] and the number of divisions along each reciprocal lattice vector was chosen such that the product of this number with the real lattice constant is 70 Å to ensure that all the enthalpy calculations are well converged to less than 1 meV per atom. The crystal orbital Hamilton populations (COHPs)[31] and the negative of the COHP integrated into the Fermi level (−ICOHP) were calculated using the LOBSTER package[32] to analyze the bonding in the crystal structures. To determine if the predicted structures were dynamically stable, phonon frequencies were calculated using direct supercell and/or density functional perturbation theory (DFPT).[33] The supercell approach uses the forces obtained by the Hellmann–Feynman theorem, as performed in PHONOPY code[34] DFPT and the electron–phonon coupling (EPC) calculations were implemented in the QUANTUM ESPRESSO program.[35] PAW pseudopotentials[29] for Cd and H elements were used with cutoff energy of 100 Ry, and the Brillouin zone sample of Methfessel–Paxton[36] using a smearing value of 0.025 Ry. We employed $12 \times 12 \times 15$ k-point grids for all of the electronic Brillouin zone integrations and $4 \times 4 \times 5$ q-meshes for all of the phonon calculations.

3. Results and discussion

In this paper, we predicted nearly 300000 prototype structures of cadmium hydrides with different stoichiometries. We find that there are no dynamically stable crystal structures in the Cd–H ratios from 1:1 to 1:4 (Figs. S1 and S2), whereas nine hitherto unknown phases (Fig. S3) are identified in the binary Cd–H system at ratios ranging from 1:5 to 1:7 (Figs. S4 and S5), within the pressure range of 100 GPa to 300 GPa., in which a novel orthorhombic structure of CdH_6 with space group *Cmcm* is found, as can be seen in Fig. 1. Experimentally, CdH_2 is the only identified compound within this system. It is a solid, known only as a thermally unstable, insoluble white powder.[37] Therefore, we choose pure cadmium and H_2 molecules as chemical precursors. Since this system is concerned with compounds that have different ratios, which could be synthesized from Cd and H_2, we analyze the two-dimensional (2D) convex hull that plots the enthalpy of formation, ΔH, from these two starting pure elements between 100 GPa and 300 GPa (Fig. S6). It is found that only CdH_6 lies on the 2D convex hull at 100 GPa. As the pressure increases up to 200 GPa, the stoichiometries that lie on the 2D convex hull are CdH_5, CdH_6 and CdH_7. By 290 GPa, the CdH_6 stoichiometry emerges as metastable. Recent reports on binary hydrides under pressure have shown that enthalpies calculated within the static-lattice approximation cannot be employed as the only predictors of synthesizability. Experimental parameters including the choice of the precursors and temperatures employed can be tuned to obtain various kinetically stable products. Therefore, a potential experimental synthesis pathway for CdH_n is proposed via the reaction $Cd + (\frac{1}{2}H_2)_n \rightarrow CdH_n$. The stable and metastable Cd–H phases are shown in Figs. S3 and 1. Figure 1(a) shows the crystal structure of the *Cmcm*-CdH_6 phase along the a-axis. It can be seen that there are 1D zigzag graphite-like hydrogenic H_6 chains in which the bond lengths between H and H atoms are 0.96 Å, while quasimolecular H_2 units also exist in the *Cmcm*-CdH_6 phase, which lie in zigzag grooves. The distance of H–H bond is 0.76 Å in H_2 units. This structural characteristic was first found in hydrogen-rich compounds. The lattice parameters of the *Cmcm*-CdH_6 phase are $a = 3.75$ Å, $b = 7.66$ Å, $c = 2.68$ Å, $\alpha = \beta = \gamma = 90$ °C at 300 GPa, respectively. The Wyckoff positions are as follows: Cd occupies 4c (0.50, 0.71971, 0.25); four inequivalent positions are identified, namely, H1 occupies 4c (0.50, 0.89610, 0.75), H2 occupies 4c (0.50, 0.99562, 0.75), H3 occupies 8g (0.23782, 0.92512, 0.25), and H4 occupies 8e (0.86584, 0.00, 0.00). The structural information of the other eight structures can be found in Table S1.

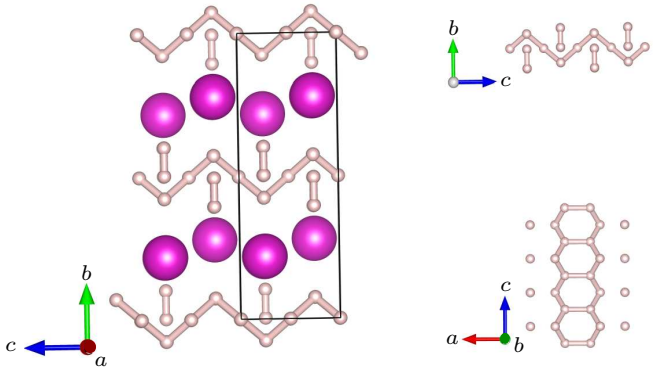


Fig. 1. High-pressure crystal structure of the *Cmcm*-CdH_6 phase along the a-axis, with the inset showing a one-dimensional chain of H_6 rings and H_2 units. The Cd (dark pink) and H (pink) atoms are represented by the colored spheres.

Figure S6 shows the phonon band structures of the *Cmcm*-CdH_6 phase at different pressures. It is found that there is no

imaginary phonon vibration in the entire Brillouin zone, indicating that the structure is dynamically stable in the pressure range from 290 GPa to 400 GPa. With increasing pressure, the acoustic phonon frequencies remain unchanged. However, the optical phonon modes obviously harden. This phenomenon may lead to the weakening of superconducting properties. Table 1 gives the elastic constants C_{ij}, bulk modulus B, shear modulus G, Young's modulus E, Poisson's ratio ν and B/G ratio of the *Cmcm*-CdH_6phase at 300 GPa. For a stable orthorhombic phase (independent elastic constants C_{11}, C_{22}, C_{33}, C_{44}, C_{55}, C_{66}, C_{12}, C_{13}, C_{23}), the criteria for mechanical stability[38] are given by

$$C_{11}>0,\ C_{22}>0,\ C_{33}>0,\ C_{44}>0,\ C_{55}>0,\ C_{66}>0,$$
$$[C_{11}+C_{22}+C_{33}+2(C_{12}+C_{13}+C_{23})]>0,$$
$$(C_{11}+C_{22}-2C_{12})>0,\ (C_{11}+C_{33}-2C_{13})>0,$$
$$(C_{22}+C_{33}-2C_{23})>0.$$

Obviously, the elastic constants of the *Cmcm*-CdH_6 phase satisfy the generalized Born mechanical stability criteria for stable orthorhombic structures, indicating that the *Cmcm*-CdH_6 phase is mechanically stable. This is in accordance with its phonon band structures (Fig. S1). To investigate its elasticity, the bulk modulus B, shear modulus G, Young's modulus E, Poisson's ratio ν and B/G ratio of *Cmcm*-CdH_6 phase are calculated from elastic constants, using the Voigt–Reuss–Hill approximation.[39] As can be seen in Table 1, the bulk modulus B is 1012.28 GPa, shear modulus G is 168.29 GPa, Young's modulus E is 478.37 GPa. This structure exhibits good compression resistance and rigidity. Meanwhile, the calculated values of the Poisson ratio and B/G ratio indicate its brittle properties. In general, when the B/G ratio is more than 1.75, the *Cmcm*-CdH_6 phase indicates excellent ductility. The value of the Poisson ratio is more than $1/3$, it exhibits ductile behavior. In the *Cmcm*-CdH_6 phase, the values of Poisson's ratio and the B/G ratio are 0.42 and 6.02, respectively. It is a typical malleable material.

Table 1. The elastic constants C_{ij}, bulk modulus B, shear modulus G, Young's modulus E, Possion ratio ν and B/G ratio of the *Cmcm*-CdH_6 phase at 300 GPa.

System	C_{11}	C_{22}	C_{33}	C_{44}	C_{55}	C_{66}	C_{12}
CdH_6	1362.82	1456.84	1242.09	124.88	454.61	89.01	834.69
Cmcm	C_{13}	C_{23}	B	G	E	ν	B/G
300GPa	899.12	807.83	1012.28	168.29	478.37	0.42	6.02

Figure 2 shows the band structures projected onto atomic orbitals (wide bands) (Fig. 2(a)) and the projected density of states (DOS) (Fig. 2(b)) at 300 GPa. It is found that the conductive bands are across the Fermi level (E_F) along the Γ–Z–T and R–Z directions, while the valence bands pass through E_F along T–Y–Γ and S–R (Fig. 2(a)), indicating the metallic nature of the *Cmcm*-CdH_6 phase. At the same time, Fig. 2(b) shows that there is a monoatomic H s state in the 1D zigzag graphite-like hydrogenic H_6 chains and the Cd p, d states are found to make the largest contributions to the DOS at E_F. Meanwhile, the H s state in the quasimolecular H_2 unit and the Cd s states slightly contribute to the diminished DOS near E_F. These results are in accordance with those of the wide bands. There are approximately twice as many hydrogen atoms in the 1D zigzag graphite-like hydrogenic H_6 chains as compared to those in the quasimolecular H_2 unit. Figure S7 shows the electronic band structures and total DOS at different pressures. With increasing pressure, the electronic bands near E_F remain unchanged, while the total DOS also remains nearly invariant. These results indicate that pressure has a minor impact on the electronic properties of the *Cmcm*-CdH_6 phase.

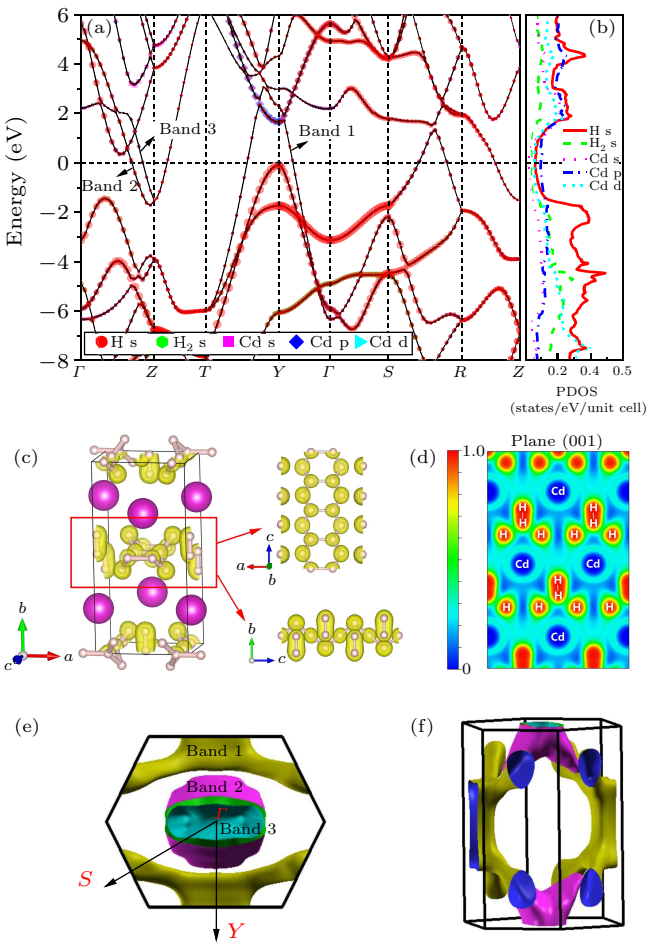


Fig. 2. Electronic structure of the *Cmcm*-CdH_6 phase at 300 GPa: (a) wide bands illustrating the characteristics arising from the monoatomic H and molecular H_2 s states, Cd s, p and d states. (b) Projected density of states at 300 GPa. The Fermi energy is set to 0 eV (dashed lines). (c) 3D electron localization function (ELF), (d) 2D ELF of plane (001). (e) and (f) Fermi surface top and side views.

In order to further confirm the bonding characteristics of the hydrogen elements in the *Cmcm*-CdH_6 structure, figure 2(c) presents the three-dimensional (3D) electron localization function (ELF) diagram of the *Cmcm*-CdH_6 phase at

300 GPa. Clearly, it can be observed that electron clouds gather around the hydrogen elements. It is evident that hydrogen elements in this orthorhombic phase exist in two forms, namely, a quasimolecular H_2 unit and monoatomic H, which forms 1D zigzag graphite-like hydrogenic H_6 chains, representing distinct charge localization modes, as can be seen inset of Fig. 2(c). Moreover, the 2D ELF on the (001) plane, which contains Cd atoms, monoatomic H and a quasimolecular H_2 unit, is depicted in Fig. 2(d). It is clearly shown that the electrons are located around the monoatomic H and quasimolecular H_2 unit. In the *Cmcm*-CdH_6 phase, there are two structural forms of hydrogen. At the same time, a metallic bond is formed between the Cd atom and monoatomic H. Compared with ordinary bonds, such as ionic or covalent bonds, the metallic bonds involve weaker interactions. However, in compounds such as metal superhydrides, this effect becomes essential for their formation and stability. Systems exhibiting such structural characteristics have the potential to become high-temperature superconductors. In addition, Figs. 2(e)–2(f) show the 3D Fermi surface viewed from the top and the side at 300 GPa, respectively. It can be found that there are three energy bands across E_F. These three bands crossing the Fermi level are labeled band 1, band 2 and band 3 in Fig. 2(a), respectively, corresponding to the three-dimensional Fermi surface (Fig. 2(e)), and distinguishes the Fermi surface pockets associated with each crossing at E_F. Meanwhile, to be clearer, we also provide the top and side views of the individual Fermi surface crossing the E_F (in Fig. S9). Evidently, there is a Fermi-nesting mechanism within the Fermi surface. This is a typical electronic feature, which usually exhibits high-temperature superconducting properties.

To further investigate if the Kubas-like mechanism occurs within the *Cmcm*-CdH_6 phase, we studied the negative of the crystal orbital Hamilton population integrated up to the Fermi level (–COHP) for selected atom pairs since it is a measure of their bond strength (Table 2). The nearest neighbor H–H bond lengths in the *Cmcm*-CdH_6 phase, 0.763 Å at 300 GPa, are somewhat longer and weaker than for pure solid hydrogen (0.756 Å) (−ICOHPs of 4.08 vs. 6.21 eV/bond). Moreover, The ICOHP of an isolated H_2 molecule with the same bond length as the H_2 unit (0.763 Å) in *Cmcm*-CdH_6 was also calculated at 300 GPa. The resulting –ICOHP value is 5.15 eV/bond, which is higher than that (4.08 eV/bond) of the H_2 unit within the *Cmcm*-CdH_6 crystal, indicating a stronger H–H interaction in the isolated H_2 molecule. These differences arise from electron donation to the H_2 anti-bonding orbital within the crystal, which weakens the interaction despite similar bond lengths. The interaction between monoatomic H atoms with the shortest distances is relatively weakened, with only 1.99 eV/bond. The interaction between Cd atoms and H atoms is even lower, at 0.70 eV/bond. The value of −COHP is positive, indicating a bonded state. Conversely, when −COHP is a negative value, it represents an antibonding state. Figure 3 shows the −COHP diagram for hydrogen with the quasimolecular H_2 unit and monoatomic H with the shortest distances in the *Cmcm*-CdH_6 phase at 300 GPa. It is evident that the occupied bonding states in *Cmcm*-CdH_6 phase occur below the Fermi level, indicating its stability. Electrons in both types of hydrogen atom units occupy certain antibonding states between H atoms. This is because when Cd atoms form hydrides with H atoms, the Cd atoms transfer electrons to the H atoms, thereby promoting the decomposition of hydrogen molecules. This will lead to electrons weakening the H–H bond by occupying antibonding orbital states, the well-known Kubas-like mechanism.[40] With increasing pressure, the bond strength remains unchanged (Fig. S8). This result is consistent with Bader charge analysis (Table S2). We present the Bader charge analysis at different pressures in Table S2. As shown in this table, the ability of the different types of atoms in the *Cmcm*-CdH_6 phase to gain or lose electrons remains largely unchanged as the pressure increases from 290 GPa to 400 GPa. At 290 GPa, cadmium loses 0.51*e*, while the H atom and H molecule obtain 0.14/0.03*e* and 0.14*e*/0.02, respectively. With the pressure increasing up to 400 GPa, cadmium still loses 0.51*e*, while the H atom and H molecule obtain 0.14/0.03*e* and 0.14/0.02*e*, respectively. It is shown that the variation of pressure has a slight impact on their bond strength, which is rare among group IIB atoms.

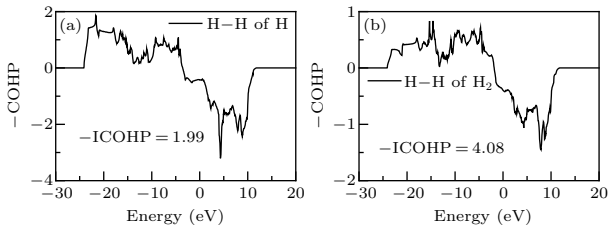


Fig. 3. The negative of the crystal orbital Hamilton population (−COHP) diagram for hydrogen of the quasimolecular H_2 unit and monoatomic H with the shortest distances in the CdH_6-*Cmcm* phase at 300 GPa.

Table 2. Distance between selected atom pairs in the *Cmcm*-CdH_6 structure and their corresponding crystal orbital Hamilton populations (−COHPs) integrated up to the Fermi level at 300 GPa.

System	Atom pairs	Distance (Å)	–ICOHP (eV/bond)
CdH_6	H–H (H in H_2 unit)	0.763	4.08 (6.21[a], 5.15[b])
Cmcm	H–H (H in atomic)	0.964	1.99
300 GPa	Cd–H	1.856	0.70

[a] The H–H distance in solid hydrogen molecular H_2 at 300 GPa is 0.756 Å, with corresponding a −COHP of 6.21 eV/bond.
[b] The H–H distance in an isolated hydrogen pair H_2 with the same bond length as the H_2 unit (0.763 Å) in *Cmcm*-CdH_6 is 0.763 Å, with the corresponding −COHP of 5.15 eV/bond.

We investigated the superconductivities of the metallic *Cmcm*-CdH_6 phase at different pressures by calculating the logarithmic average phonon frequencies $\langle\omega_{log}\rangle$, EPC constant

λ, the electronic density of states $N(E_F)$ at the Fermi level and superconductive critical temperature T_c (Table 3). At 290 GPa, the $\langle\omega_{log}\rangle$ of the *Cmcm*-CdH_6 phase is 440.50 K and the EPC parameter λ is 1.16. $\langle\omega_{log}\rangle$ is monotonically increasing, while the λ values monotonically decrease as the pressure increases. Using the Allen–Dynes-modified McMillan equation, its T_c values are 37.6–29.1 K with the Coulomb pseudopotential $\mu^* = 0.1$ in the pressure range from 290 GPa to 400 GPa. When $\mu^* = 0.13$, its T_c values are 33.1–20.6 K. Notably, a possible reason for this is the complex influence of compression on the phonon frequencies. However, the pressure has a negligible impact on the electronic structure around the Fermi level, which basically remains unchanged. The similar DOS behavior ($N(E_F)$) under different pressures implies a minor influence of electronic properties on superconductivity. Moreover, the variant relationship of the T_c values is also investigated with varying pressures. As can be seen in Table 3, this results in the T_c values of the *Cmcm*-CdH_6 phase also diminishing. At the minimum stabilizing pressure, it achieves its maximum T_c value, i.e., 37.6 K at 290 GPa. It is well-known that for strongly coupled systems, this method underestimates the value of T_c. Numerically solving the Eliashberg equations provides a more accurate estimate, resulting in values as high as 58.9 K at 290 GPa, an improvement of 56.6% (see Fig. 4(d)). Moreover, we try to understand how the hydrogenic motifs in the *Cmcm*-CdH_6 phase influence the EPC and the predicted T_c value. We compare the superconducting properties of *Cmcm*-CdH_6 (37.6 K, 290 GPa) with non-clathrate scandium hydrides,[41,42] including *P6/mmm*-ScH_2 (4 K, 300 GPa), *P6*$_3$*/mmc*-ScH_3 ($<$ 1 K, 400 GPa), *I4/mmm*-ScH_4 (68 K, 250 GPa) and *P6*$_3$*/mmc*-ScH_6 (29 K, 250 GPa), in the pressure range of 250–400 GPa. None of these compounds exhibit high T_c. Similar to the non-clathrate scandium hydrides,[41,42] the *Cmcm*-CdH_6 phase contains H_2 units within its structure, which could suppress the electronic DOS at the Fermi level and, consequently, hinder the realization of high T_c. It has been noted that this phenomenon occurs under similar conditions;[41] specifically, high-pressure hydrides with large predicted T_c typically feature a hydrogenic lattice lacking quasi-molecular H_2 or H_3^- units, as the electronic structure of such systems is only weakly affected by the vibrations of the H atoms.

Table 3. The calculated EPC parameter (λ), logarithmic average phonon frequency ($\langle\omega_{log}\rangle$, K), superconductive critical temperature with $\mu^* = 0.1$ (T_c, K), and the electronic density of states at the Fermi level ($N(E_F)$, states/spin/Ry/unit cell) for the *Cmcm*-CdH_6 phase and various scandium hydrides under compression.

System	P (GPa)	$\langle\omega_{log}\rangle$ (K)	λ	T_c (K) ($\mu^* = 0.1$)	$N(E_F)$
Cmcm-CdH_6 Our work	290	440.5	1.16	37.6	2.85
	300	926.1	0.74	37.2	2.84
	350	1183.3	0.62	29.8	2.82
	400	1232.3	0.61	29.1	2.81
P6/mmm-ScH_2 [41,42]	300	543.5	0.44	4	
P6$_3$*/mmc*-ScH_3 [41,42]	400	571.8	0.17	<1	
I4/mmm-ScH_4 [41,42]	250	1891.8	0.81	68	
P6$_3$*/mmc*-ScH_6 [41,42]	250	1439.8	0.57	29	

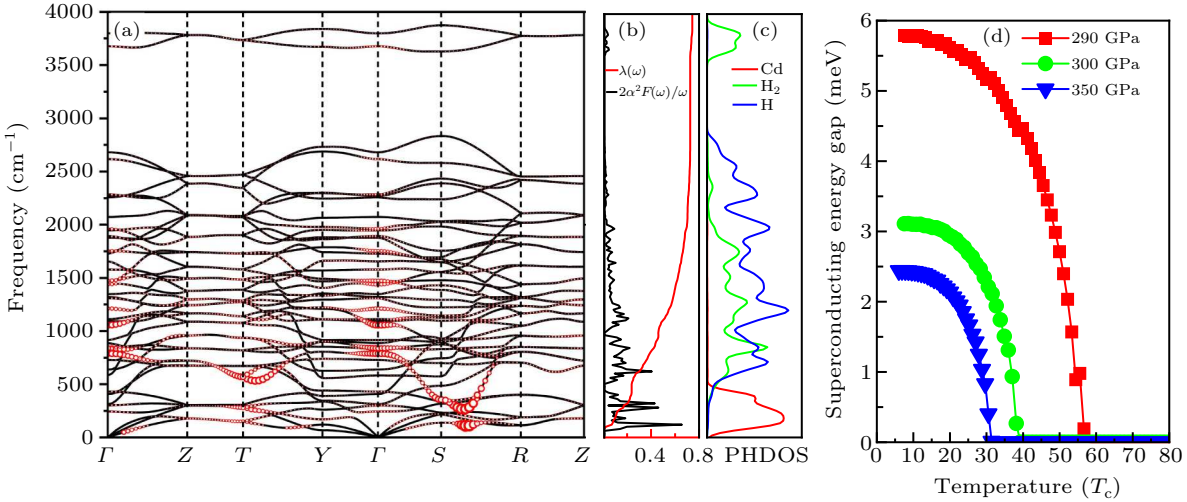


Fig. 4. Superconducting properties of *Cmcm*-CdH_6 at 300 GPa. (a) Phonon dispersion curves, where the area of the red circles is proportional to the electron–phonon coupling parameter, λ_{qv}, for mode v at wavevector q (phonon linewidth). (b) The Eliashberg spectrum function (black line) and the electron–phonon integral, $\lambda(\omega)$ (red solid line). (c) The projected phonon density of states (PHDOS). The blue line represents monoatomic H in 1D zigzag graphite-like hydrogenic H_6 chains and the green line represents H in the quasimolecular H_2 unit. (d) Superconducting energy gaps at different pressures.

To further reveal the superconductive mechanism of the *Cmcm*-CdH_6 phase, Figure 4 shows the phonon dispersions, the projected phonon density of states (PHDOS), the Eliashberg spectral function $\alpha^2F(\omega)$ and the electron–phonon coupling constant integral $\lambda(\omega)$ for the *Cmcm*-CdH_6 phase at 30 GPa, respectively. A notable indication of the existence of two typical hydrogen configurations in the structure is the separation of the vibrational modes into two significantly distinct regions (Fig. 4(a)), namely, the lower and intermediate frequencies are grouped together, and distinct from the higher-

frequency region. The lower frequencies (below 0–500 cm^{-1}) are associated with the heavier Cd atoms. The intermediate frequencies (ranging from 500 cm^{-1} to 2856 cm^{-1}) arise from the combination of hydrogen atoms in the quasimolecular H_2 unit and monoatomic hydrogen which forms 1D zigzag graphite-like hydrogenic H_6 chains. The higher frequencies (between 3580 cm^{-1} and 3930 cm^{-1}) are derived completely from the contribution of hydrogen atoms in the quasimolecular H_2 unit. In this structure, the two phonon frequency regions contribute 97.7%, in which the contribution from Cd atoms constitutes approximately 32.5%, and the combined interaction of H atoms in the H_2 unit and monoatomic H atoms contributes 65.2% and 2.3% to the total λ values, respectively, as can been seen in Figs. 4(b) and 4(c). In the *Cmcm*-CdH_6 phase, the greatest contributions (the area of red circles) to electron–phonon coupling constant (λ) are in *Z*–*T*–*Y* and Γ–*S*–*R*, which are two high symmetry directions. The contribution of the Γ–*S*–*R* direction to the electron–phonon coupling constant (λ) primarily arises from the Cd atoms. In the *Z*–*T*–*Y* direction, the contribution to the electron–phonon coupling constant (λ) mainly originates from the collective effect of H atoms in the quasimolecular H_2 unit and monoatomic H atoms. The superconductivity of the *Cmcm*-CdH_6 structure primarily arises from the cooperative interaction of two types of hydrogen atoms forming bonds in the intermediate frequency region. Figure 4(d) presents the superconducting energy gap diagram of the *Cmcm*-CdH_6 phase under different pressures. It can be observed that its T_c value is estimated to be 58.9 K using the superconducting energy gap equation, surpassing the value of 37.6 K estimated by the McMillan equation. This discrepancy may be attributed to the anisotropy. With increasing pressure, the value of T_c decreases, which is consistent with the results estimated by the McMillan equation.

4. Conclusion and perspectives

In summary, structural predictions have identified nine hitherto unknown phases with unique stoichiometries in the binary Cd–H system in the range of 100–300 GPa. We have extensively explored the structural and dynamical stability, as well as the electronic and superconducting properties, of cadmium hydrides at high pressure. We found that the low-energy structures of the binary cadmium hydrides exhibit very low spatial symmetry. Moreover, the metallic *Cmcm*-CdH_6 phase was found to be both dynamically and mechanically stable above 290 GPa. This structure exhibits excellent ductility, resistance to compression, and rigidity. The structural characteristics of the one-dimensional H_6 ring forming a folded zigzag chain were first observed in the *Cmcm*-CdH_6 structure, which is metastable between 290 GPa and 400 GPa. The shortest H–H bond slightly increases compared to that in molecular H_2, while the other H–H bond lengths show a significant increase. This is primarily attributed to the charge transfer from H_2 $\sigma \rightarrow$ Cd d donation and Cd d $\rightarrow$ H_2 σ^* back-donation via the Kubas-like mechanism. The DOS at E_F is mainly contributed by H s, Cd p and d, and it remains constant with increasing pressure. The Fermi surface is nearly invariant across the range of dynamic stability. Electrons transferred from Cd atoms to H atoms occupy antibonding orbitals for both types of hydrogen atoms. This weakens the strength of chemical bonds, promoting the emergence of superconductivity. The T_c value of the *Cmcm*-CdH_6 phase calculated via the Allen–Dynes-modified McMillan equation is 37.6 K at 290 GPa, which decreases with increasing pressure from 37.6 K to 29.1 K. Numerically solving the Eliashberg equation yields a higher T_c value of 58.9 K at 290 GPa. Our work provides a new understanding of the high-pressure phase transition sequences and superconducting mechanism in the *Cmcm*-CdH_6 phase. It promotes the search for novel hydrides and exploration of the superconductivity properties of 1D zigzag graphite-like hydrogenic H_6 chains and quasimolecular H_2 units. We are looking forward to future work studying the effect of chemical substitution on the stability and superconducting properties of phases with group IIB elements under compression.

Acknowledgments

Project supported by the Jilin Provincial Natural Science Foundation (Grant No. 20230101183JC) and the Center for Computational Research at Jilin Province.

References

[1] Cui W W, Bi T G, Shi J M, Li Y W, Liu H Y, Zurek E and Hemley R J 2020 *Phys. Rev. B* **101** 134504
[2] Drozdov A P, Eremets M I, Troyan I A, Ksenofontov V and Shylin S I 2015 *Nature* **525** 73
[3] Drozdov A P, Kong P P, Minkov V S, Besedin S P, Kuzovnikov M A, Mozaffari S, Balicas L, Balakirev F F, Graf D E, Prakapenka V B, Greenberg E, Knyazev D A, Tkacz M and Eremets M I 2019 *Nature* **569** 528
[4] Liang X W, Wei X D, Zurek E, Bergara A, Li P F, Gao G Y and Tian Y J 2024 *Matter Radiat. Extrem.* **9** 018401
[5] Ma L, Wang K, Xie Y, Yang X, Wang Y Y, Zhou M, Liu H Y, Yu X H, Zhao Y S, Wang H B, Liu G T and Ma Y M 2022 *Phys. Rev. Lett.* **129** 269901
[6] Flores-Livas J A, Boeri L, Sanna A, Profeta G, Arita R and Eremets M I 2020 *Phys. Rep.* **856** 1
[7] Li Y H, Zhou P, Ding C, Lu Q, Wang X M and Sun J 2024 *Chin. Phys. B* **33** 106102
[8] Cui W W and Li Y W 2019 *Chin. Phys. B* **28** 107104
[9] Ashcroft N W 1968 *Phys. Rev. Lett.* **21** 1748
[10] Hilleke K P and Zurek E 2022 *J. Appl. Phys.* **131** 070901
[11] Ashcroft N W 2004 *Phys. Rev. Lett.* **92** 187002
[12] Sun W G, Chen B L, Li X F, Peng F, Hermann A and Lu C 2023 *Phys. Rev. B* **107** 214511
[13] Yan X Z, Zhou X Z, Liu C F, Xu Y L, Huang Y B, Sheng X W and Chen Y M 2024 *Chin. Phys. B* **33** 086301
[14] Gao G, Wang L, Li M, Zhang J, Howie R T, Gregoryanz E, Struzhkin V V, Wang L and Tse J S 2021 *Mater. Today Phys.* **21** 100546
[15] Einaga M, Sakata M, Ishikawa T, Shimizu K, Eremets M I, Drozdov A P, Troyan I A, Hirao N and Ohishi Y 2016 *Nat. Phys.* **12** 835

[16] Somayazulu M, Ahart M, Mishra A K, Geballe Z M, Baldini M, Meng Y, Struzhkin V V and Hemley R J 2019 *Phys. Rev. Lett.* **122** 027001

[17] Liu H Y, Naumov I I, Hoffmann R, Ashcroft N W and Hemley R J 2017 *Proc. Natl. Acad. Sci. USA* **114** 6990

[18] Wang H, Tse J S, Tanaka K, Iitaka T and Ma Y 2012 *Proc. Natl. Acad. Sci. USA* **109** 6463

[19] Jeon H, Wang C, Liu S, Bok J M, Bang Y and Cho J H 2022 *New J. Phys.* **24** 083048

[20] Li Z W, He X, Zhang C L, Wang X C, Zhang S J, Jia Y T, Feng S M, Lu K, Zhao J F, Zhang J, Min B S, Long Y W, Yu R C, Wang L H, Ye M Y, Zhang Z S, Prakapenka V B, Chariton S, Ginsberg P A, Bass J, Yuan S H, Liu H Z and Jin C Q 2022 *Nat. Commun.* **13** 2863

[21] Semenok D V, Kvashnin A G, Ivanova A G, Svitlyk V, Fominski V Y, Sadakov A V, Sobolevskiy O A, Pudalov V M, Troyan I A and Oganov A R 2020 *Mater. Today* **33** 36

[22] Snider E, Dasenbrock-Gammon N, McBride R, Wang X Y, Meyers N, Lawler K V, Zurek E, Salamat A and Dias R P 2021 *Phys. Rev. Lett.* **126** 117003

[23] Troyan I A, Semenok D V, Kvashnin A G, Sadakov A V, Sobolevskiy O A, Pudalov V M, Ivanova A G, Prakapenka V B, Greenberg E, Gavriliuk A G, Lyubutin I S, Struzhkin V V, Bergara A, Errea I, Bianco R, Calandra M, Mauri F, Monacelli L, Akashi R and Oganov A R 2021 *Adv. Mater.* **33** 2006832

[24] Kong P P, Minkov V S, Kuzovnikov M A, Drozdov A P, Besedin S P, Mozaffari S, Balicas L, Balakirev F F, Prakapenka V B, Chariton S, Knyazev D A, Greenberg E and Eremets M I 2021 *Nat. Commun.* **12** 5075

[25] Wang Y, Lv J, Zhu L and Ma Y 2010 *Phys. Rev. B* **82** 094116

[26] Wang Y, Lv J, Zhu L and Ma Y 2012 *Comput. Phys. Commun.* **183** 2063

[27] Kresse G and Fu J 1996 *Phys. Rev. B* **54** 11169

[28] Kresse G and Joubert D 1999 *Phys. Rev. B* **59** 1758

[29] Blöchl P E 1994 *Phys. Rev. B* **50** 17953

[30] Monkhorst H J and Pack J D 1976 *Phys. Rev. B* **13** 5188

[31] Dronskowski R and Blöchl P E 1993 *J. Phys. Chem.* **97** 8617

[32] Maintz S, Deringer V L, Tchougréeff A L and Dronskowski R 2013 *J. Comput. Chem.* **34** 2557

[33] Gonze X and Lee C 1997 *Phys. Rev. B* **55** 10355

[34] Togo A, Oba F and Tanaka I 2008 *Phys. Rev. B* **78** 134106

[35] Giannozzi P, Baroni S, Bonini N, Calandra M, Car R, Cavazzoni C, Ceresoli D, Chiarotti G L, Cococcioni M and Dabo I 2009 *J. Phys.: Condens. Matter.* **21** 395502

[36] Methfessel M and Paxton A T 1989 *Phys. Rev. B* **40** 3616

[37] Barbaras G D, Dillard C, Finholt A E, Wartik T, Wilzbach K E and Schlesinger H I 1951 *J. Am. Chem. Soc.* **73** 4585

[38] Wu Z J, Zhao E J, Xiang H P, Hao X F, Liu X J and Meng J 2007 *Phys. Rev. B* **76** 054115

[39] Hill R 1952 *Proc. Phys. Soc. A Lond.* **65** 349

[40] Kubas G J, Ryan R R, Swanson B I, Vergamini P J and Wasserman H J 1984 *J. Am. Chem. Soc.* **106** 451

[41] Ye X, Zarifi N, Zurek E, Hoffmann R and Ashcroft N W 2018 *J. Phys. Chem. C* **122** 6298

[42] Peng F, Sun Y, Pickard C J, Needs R J, Wu Q and Ma Y M 2017 *Phys. Rev. Lett.* **119** 107001